The International Journal of Advanced Manufacturing Technology (2019) 100:577–588
https://doi.org/10.1007/s00170-018-2709-z

ORIGINAL ARTICLE

Prediction of cutting force of ball-end mill for pencil-cut machining

Z. C. Wei[1] · M. L. Guo[1] · M. J. Wang[1] · S. Q. Li[1] · S. X. Liu[1]

Received: 6 June 2018 / Accepted: 17 September 2018 / Published online: 26 September 2018

Abstract
There are a number of concave circular blending surfaces with minor curvature radius in the corner of curved surface part, like complex mold cavity. Pencil-cut machining has shorter path and completer material remove than other strategies of clean-up machining which make it high efficiency, high precision, and high utilization rate of equipment. In this paper, contact between cutter and concave crescent cylinder (CCC) including cutter workpiece engagement (CWE) and in-cut cutter edge (ICCE) is studied based on an analytic method, and a prediction model of the cutting force for pencil-cut machining with the ball-end mill is established. The cutter, the CCC, and the feed direction for pencil-cut machining are parametrically defined. In cutter contact normal coordinate system, the analytic expressions of tool geometry, CCC, and the cutter sweep surface of the cutter are derived, and then the CWE is obtained by the intersection of the space surfaces, which the CWE in the tool coordinate is realized by the three-dimensional rotation transformation. The cutter edge curve is discreted into a series of infinitesimal element, based on the criteria of the cutter edge element in the CWE, an analytic algorithm to calculate the ICCE is proposed, and the precision of the boundary points can be further improved by the dichotomy. Combining ICCE with instantaneous chip thickness considering cutter run-out and micro-element milling force theories of ball-end mill, the prediction model of cutting force for pencil-cut machining of CCC with ball-end mill is established. A series of pencil-cut machining experiments and simulations were arranged. The performance of pulling milling is better than that of pushing milling. The CWE and ICCE obtained by the analytical method agree well with that of experiment and solid modeling simulation. The cutting force experiments verify the correctness of the milling force predictive model.

Keywords Pencil-cut machining · Cutting force prediction · Cutter workpiece engagement (CWE) · In-cut cutter edge (ICCE) · Ball-end mill · Cutter run-out

1 Introduction

Parts with complex surface are used much widely in aerospace, energy, chemical industry, and so on. Generally, complex surface comprises many curve surfaces. Then there are a number of concave arc corners with little diameter in the engagement of the surface blocks. The strategies of clean-up machining include pencil-cut, multilayer fillet-cut, contouring clean-up, suturing clean-up, and automatic clean-up. Because of the small diameter, the long toolbar, and the weakly rigidity, as well as the large chipping allowance and the unevenly distribution in clean-up machining, it vibrates easily in the machining process. Actually, the conservative cutter path and cutting parameter are applied in the production, like multilayer fillet-cut and contouring clean-up, which cause a great waste of equipment and seriously affect the machining efficiency and manufacturing cost. For pencil-cut machining, because it has the advantage of the continuous path and the shortest length, material can be removed completely in theory. It is the ideal choice for corner clean up. The main reason of pencil-cut machining's difficult popularity is the lack of research on its cutting mechanical mechanism. Cutting force is the direct inducement of vibration of machining system, and it has great influence on tool wear, workpiece deformation, and so on. In the process of the mechanics modeling for pencil-cut machining, the relationship of the cutter relative to the workpiece and the feed direction is arbitrary, and a proper parameter definition is required. The contact between cutter and

✉ Z. C. Wei
wei_zhaocheng@dlut.edu.cn

[1] Key Laboratory for Precision and Non-traditional Machining Technology of Ministry of Education, Dalian University of Technology, Dalian 116024, People's Republic of China

workpiece changes continuously with the tool axis vector, machining parameters, and workpiece geometry, and it is necessary to establish a model for accurate and real-time description. The cutting force coefficients have size effect [1], and the ball-end mill coefficients are also related to the axial factor [2]. Because of the cutter run-out, the effective cutting radius of the cutter edge also changes [3]. In addition, the cutter edge segment that actually participates in the cutting reflects the thickness of the undeformed chip and is the key to the prediction of the cutting force. The above points are the current difficulties in achieving cutting force prediction.

Scholars have also done a lot of analysis on corner processing in the cavity. Park et al. [4] and Choy et al. [5] used the extended pair-wise interference-detection offset algorithm and the method of adding Bow-like tool path segments respectively to optimize the tool path of the corner pocket machining for realizing the removal of the residual material. Pateloup et al. [6] analyzed the influence of the tool path of the corner pocket machining on the kinematics characteristics, reduced the cutting time, and increased the feed rate by optimizing the curvature radius of tool path in corner. Bouaziz et al. [7] developed an analytical model to calculate tool path length and cutting time for pocket machining including corner areas, then maximized efficiency by optimizing tool size selection. Aiming at pocket milling, Guerrero-villar et al. [8] proposed that the tool geometry was represented by the circular parameter equation and the processed area was represented by the superposition of tool geometries of different cutter position points, thereupon put forward an algorithm of CWE by finding the intersection of them. Zhang et al. [9] discretized the corner machining along the tool path into a series of steady-state machining with different radial cutting depth and proposed the analytic models of cutting depth, contact angle, feed per tooth, and average chip thickness at different discrete points. Whereafter, the cutting force prediction for corner machining was established. In the corner pocket machining, Law et al. [10] believed that the varying radial cutting depth leaded to the machining error constantly change because of its influence on cutting force. Then they established an error prediction model for corner groove and small radial cutting depth machining. Based on the cutting force model of corner pocket machining, Dotcheva et al. [11] deduced the error prediction equation of the corner machining with carrying out the two-step cantilever beam analysis of the tool, achieving high-precision machining by adjusting the feed rate. Bae et al. [12] established a simple and novel mechanical model suitable for corner pocket machining based on the tool workpiece contact angle, cutting depth, and feed rate. The cutting-load regularization method proposed can change the feed rate to control the milling force within the safety range. Peng et al. [13] put forward a dynamic model based on the time-domain simulation algorithm for circular corner machining, then obtained machining stability lobe diagrams by solving the differential equation with implicit three-step four-order ADAMS numerical analysis method. The above researches on corner machining are mainly based on two-dimensional planar milling of flat-end cutter.

The literatures about the pencil-cut machining of ball-end mill mainly focus on tool path planning and tool axis vector control. Ren et al. [14] presented a tool diameter shrink method to determine the tool path of multilayer fillet-cut machining. A surface could be formed by the contact points between a series of auxiliary tools of decreasing diameter and the workpiece surface. The cutter path surface of multilayer fillet-cut machining was formed by offsetting the radius R of the cutter along the surface norm. Kim et al. [15] offset the clean-up flank and planed the tool path of pencil-cut and multilayer fillet-cut by obtaining the sharp-concave points and wall-contact vector. Determining the search initial point and search direction of pencil-cut machining, Ttang et al. [16] calculated tool path on the condition that the distance between the point and the two clean-up flanks is equal to the tool radius R. Further multilayer fillet-cut path can be obtained by changing the tool radius. Zhu et al. [17] studied the cutter axis vector of pencil-cut and developed the interference avoidance haptic induction device of the tool system by the collection and feedback of force signals with two-phase descriptive method and Dexel-based modeling method.

It is scarce in the research on prediction of cutting force for clean-up machining of ball-end mill. Aiming at two flank planes perpendicular to each other, Ding et al. [18] studied the start and exist angles of corner machining and established an analytical prediction model of cutting force. Yue et al. [19] established a three-dimensional finite element force prediction model for the mold corner milling and analyzed the variation rule of the cutting force of the corner machining.

In this paper, aiming at pencil-cut machining of ball-end mill, the cutting force prediction model is established. The general thought is shown in Fig. 1. According to the parametric definition of pencil-cut machining in the concave crescent cylinder (CCC), the analytical model of cutter workpiece engagement (CWE) is established by intersecting space surfaces.

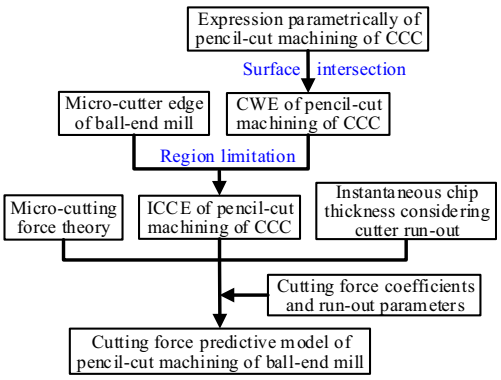

Fig. 1 Overall thinking

Further, by defining the conditions of the micro-cutter edge in the CWE, an analytic algorithm of the in-cut cutter edge (ICCE) is proposed. Combining the micro-element cutting force of the ball-end mill, the instantaneous chip thickness theory, the cutting force coefficients and the cutter run-out parameters obtained by experiments, the prediction model of the cutting force for the pencil-cut machining of ball-end mill is established finally.

2 Parameterization of geometric model of pencil-up machining

In this section, three-axis pencil-cut machining of ball-end mill is used as the analytic object. As shown in Fig. 2a, the cutting allowance of pencil-cut is the residual material of the large-diameter cutter in the previous process. The distribution of the chipping allowance will change in a crescent-like manner if the diameter of the cutter in the previous process changes gradually, and the arc at arbitrary intermediate position remains in tangent constraint with the boundary lines. The shape of the section of chipping allowance can be regarded as linear affine sweep from the inscribed arc of the plane included angle.

As shown in Fig. 2b, the characteristic parameters of CCC are defined as follows: The field angle β of the allowance cross section determines the distribution of the cutting allowance in cross section. The feeding direction $\boldsymbol{f}$ is parallel to the generatrix of CCC surface. The intersection of the cutting allowance cross section and the angular bisector is defined as the cutter contact normal $\boldsymbol{n}$. The spherical center of the ball-end mill is defined as the origin O of the cutter contact point normal coordinate system $X_nY_nZ_n$ and cutter coordinate system $X_cY_cZ_c$; Z_n-axis is along the $\boldsymbol{n}$; Y_n-axis is the same of feed direction $\boldsymbol{f}$; the X_n-axis is obtained by the right-hand rule. Z_c-axis is upward along the cutter axis. The X_c-axis is obtained by the cross product of cutter axis vector $\boldsymbol{p}$ and the contact normal $\boldsymbol{n}$. The Y_c-axis is obtained by the right-hand rule too. The static programming coordinate system is defined as the workpiece coordinate system $X_wY_wZ_w$. The included angle of the cutter axis $\boldsymbol{p}$ and cutter contact normal $\boldsymbol{n}$ is defined as the cutter axis tilt angle ε, ranging from 0 to $\pi/2$. Define the angle between the X_c-axis of the cutter coordinate system and feed direction $\boldsymbol{f}$ as the feed direction angle γ, range from 0 to π, they are shown in Eq. (1).

$$\begin{aligned}\varepsilon &= \arccos\left(\frac{\mathbf{n}g\mathbf{p}}{|\mathbf{n}\|\mathbf{p}|}\right)\\ \gamma &= \arccos\left(\frac{(\mathbf{p}\times\mathbf{n})g\mathbf{f}}{|\mathbf{p}\times\mathbf{n}\|\mathbf{f}|}\right)\end{aligned} \tag{1}$$

3 CWE analytic modeling of pencil-cut machining

In the pencil-cut machining, the radius R of the cutter is equal to the radius of the arc at the surface root, and the position relation of the CCC relative to the cutter is arbitrary. As shown in Fig. 3, the ball-end mill being regarded as a spherical surface, the area where the cutter and workpiece overlap is CWE. It is a part of sphere, consisting of two boundaries that are the circular segment AB and the space complex curve segment $(AB)'$. Based on the space geometry theory, the problem of analytical modeling of the cutter workpiece contact interface can be transformed into the intersection of the surfaces.

3.1 Analytic expressions of boundary curves in the normal coordinate system O-$X_nY_nZ_n$

With the known analytical expressions of the surfaces, the analytical equations of the boundary curves of the CWE can be obtained by the intersection calculation of the curved surfaces. The expressions of relevant surfaces in O-$X_nY_nZ_n$ are concise, convenient for calculation; hence, the analysis of the boundary curves AB, (AB)' and points A, B are derived in the coordinate system, as follows:

The boundary curve AB is the intersection of allowance section H through the spherical center O and the machined

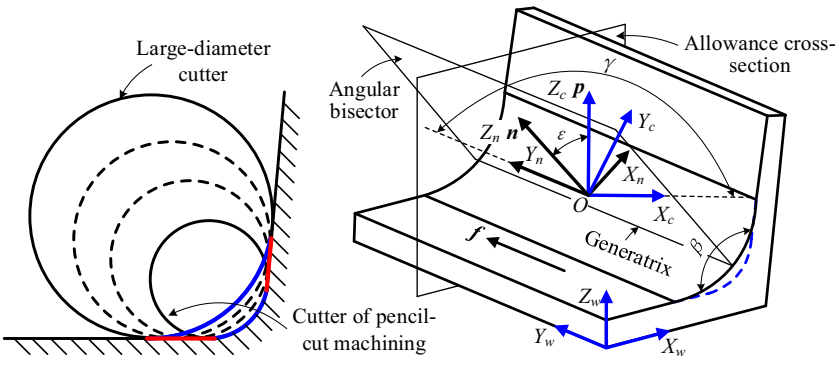

Fig. 2 Pencil-cut machining in the CCC surface. **a** Crescent-like cutting allowance. **b** Surface of CCC

surface M (the arc surface in the root of the surface). It is expressed in $O\text{-}X_nY_nZ_n$ as follows:

$$\begin{cases} y = 0 \\ x^2 + z^2 = R^2 \end{cases} \tag{2}$$

The endpoints A and B of the boundary curves AB, (AB)' are the intersection points of the sphere, the allowance section H through the spherical center and the to-be-machined arc surface N. That is, the intersections of the two arcs of radii R and R' in the plane $O\text{-}X_nZ_n$, respectively. The analytical expression is:

$$\begin{cases} x^2 + z^2 = R^2 \\ y = 0 \\ x^2 + \left[z - \left(R' + d_n - R\right)\right]^2 = \left(R'\right)^2 \end{cases} \tag{3}$$

where R' is the radius of the arc surface to be machined, namely the radius of the large-cutter. d_n is the normal cutting depth. As shown in Fig. 3b, the relationship expression between the arc radius R' and the cutting depth d_n is:

$$\left(R' - R\right)\left[\csc(\beta/2) - 1\right] = d_n \tag{4}$$

The coordinates of two intersections A and B can be derived by solving the Eq. (3) as follows:

$$\begin{aligned} &\left[x_{A(B)} \;\; y_{A(B)} \;\; z_{A(B)}\right] = \left[\pm\sqrt{R^2 - \left(\left(R^2 - \left(R'\right)^2 + T^2\right)/(2T)\right)^2} \quad 0 \quad R^2 - \left(R'\right)^2 + T^2/(2T)\right] \\ &T = R' + d_n - R \end{aligned} \tag{5}$$

In the equation, T is intermediate variable. When the sign is "-," it is the coordinate of point A. When taking "+," it is the coordinate of point B.

The boundary curve (AB)' is the intersection of the to-be-machined surface N with spherical surface. It is expressed in $O\text{-}X_nY_nZ_n$ as follows:

$$\begin{cases} x^2 + \left[z - \left(R' + d_n - R\right)\right]^2 = \left(R'\right)^2 \\ x^2 + y^2 + z^2 = R^2 \end{cases} \tag{6}$$

As shown in Fig. 3b, there is material residue between the two tool paths in machining. The scallop-height e is the distance from point B to line l in the pencil-cut machining:

$$e = x_B\cos(\beta/2) + z_B\sin(\beta/2) + R \tag{7}$$

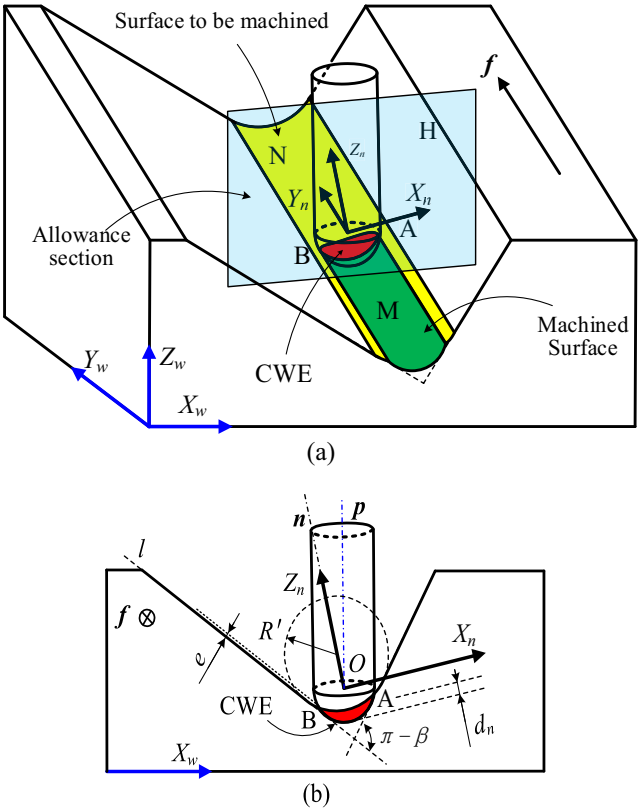

Fig. 3 The CWE of pencil-cut machining of ball-end mill. **a** 3D graph. **b** Y_n-axial view

3.2 Rotation transformation of boundary curves between coordinate systems

To establish the model of cutting force, it is necessary to obtain the CWE in the cutter coordinate system. The above expression of CWE is based on the cutter contact point normal coordinate system, and it needs to be transformed into the cutter coordinate system by the space rotation transformation. The characteristics of the two coordinate systems are as follows: the X_c-axis of the cutter coordinate system is in the X_n-Y_n plane of the cutter contact point normal coordinate system; the angle between the Z_n-axis and the Z_c-axis is ε; the angle between the X_c-axis and the Y_n-axis isγ. In the cutter contact point normal coordinate system, it is supposed that P (x_n y_n z_n) is the coordinate expression of any point in CWE. As shown in Fig. 4, the corresponding coordinate expression P (x_c y_c z_c) of this point in cutter coordinate system is obtained

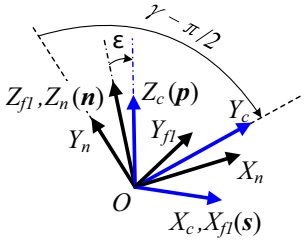

Fig. 4 Spatial rotation transformation of the coordinate system

through two rotation transformation. First rotate O-$X_nY_nZ_n$ angle γ-$\pi/2$ around the Z_n-axis to obtain the auxiliary coordinate system O-$X_{f1}Y_{f1}Z_{f1}$. Then rotate O-$X_{f1}Y_{f1}Z_{f1}$ angle ε around the X_{f1}-axis that is X_c-axis. The transformation expression is as follows:

$$\begin{cases} [x_c \quad y_c \quad z_c] = [x_n \quad y_n \quad z_n]\boldsymbol{T}_{\mathbf{n}}(\gamma-\pi/2)\boldsymbol{T}_{\mathbf{s}}(\varepsilon) \\ \boldsymbol{n} = (0 \quad 0 \quad 1); \boldsymbol{s} = (1 \quad 0 \quad 0) \end{cases} \tag{8}$$

where take $\boldsymbol{T}_{\boldsymbol{s}}(\varepsilon)$, representing the rotation angle ε around the vector $\boldsymbol{s}$, as an example to illustrate the transformation matrix format. Assuming $\boldsymbol{s} = (s_x\ s_y\ s_z)$, then the expression of $\boldsymbol{T}_{\boldsymbol{s}}(\varepsilon)$ is as follows:

$$\boldsymbol{T}_{\boldsymbol{s}(\varepsilon)} = \begin{bmatrix} s_x^2 + (1-s_x^2)\cos\varepsilon & s_x s_y(1-\cos\varepsilon) + s_z\sin\varepsilon & s_x s_z(1-\cos\varepsilon) - s_y\sin\varepsilon \\ s_x s_y(1-\cos\varepsilon) - s_z\sin\varepsilon & s_y^2 + (1-s_y^2)\cos\varepsilon & s_y s_z(1-\cos\varepsilon) + s_x\sin\varepsilon \\ s_x s_z(1-\cos\varepsilon) + s_y\sin\varepsilon & s_y s_z(1-\cos\varepsilon) - s_x\sin\varepsilon & s_z^2 + (1-s_z^2)\cos\varepsilon \end{bmatrix} \tag{9}$$

The boundary curves of CWE in cutter contact point normal coordinate system are regarded as a series of point sets, then CWE in cutter coordinate system can be obtained from the above rotation transformation.

4 ICCE of pencil-cut machining

The segment of cutter edge curve in CWE is ICCE, which is the segment that actually participates in material cutting, also defines the width of the undeformed chip layer. In this section, based on the obtained CWE, proposed the ICCE analysis algorithm of pencil-cut machining with ball-end mill by intersecting the boundary curves of the CWE and cutter edge curve.

For example, the constant lead helical ball-end mill with dextral cutter edge. The coordinate analytic expression of the micro-cutter edge located on the cutter edge curve j is [20]:

$$\begin{cases} X_j = R\sin k\sin(\psi - \varphi(k)) \\ Y_j = R\sin k\cos(\psi - \varphi(k)) \\ Z_j = -R\cos k \end{cases} \tag{10}$$

where k is the axial position angle corresponding to the micro-cutter edge, ψ is the cutter rotation position angle, α is cutter edge helix angle, and θ_j is the radial position angle corresponding to the micro-cutter edge. φ is the lag angle which indicates the delay of micro-cutter edge relative to the tip of the cutter edge. It is expressed as Eq. (11). The definitions of related parameters are shown in Fig. 5.

$$\varphi(k) = (\mathrm{j}-1)2\pi/N + (1-\cos k)\tan\alpha \tag{11}$$

As shown in Fig. 6, there are two cases where the cutter edge curve intersects with the CWE: both the upper and lower boundary points k_u and k_d of the cutter edge interval are on the boundary curve AB or point k_u is located on the boundary curve (AB)' and point k_d is located on the boundary curve AB. The cutter edge curve is discretized into a series of micro-cutter edges. For any micro-cutter edge Q ($x_c\ y_c\ z_c$) of the cutter edge in the CWE, the following two conditions need to be satisfied: (1) The micro-cutter edge Q ($x_c\ y_c\ z_c$) is within the range of the radial position angle defined by the endpoints A and B of the boundary curve. (2) The micro-cutter edge Q ($x_c\ y_c\ z_c$) is within the range of the axial position angle defined by boundary curves (AB)' and AB. In order to simplify calculation, the discretized micro-cutter edge Q ($x_c\ y_c\ z_c$) is inversely operated by the rotation transformation, using Eq. (8) to obtain the coordinate of the micro-cutter edge Q ($x_n\ y_n\ z_n$) in cutter contact normal coordinate system. In combination with

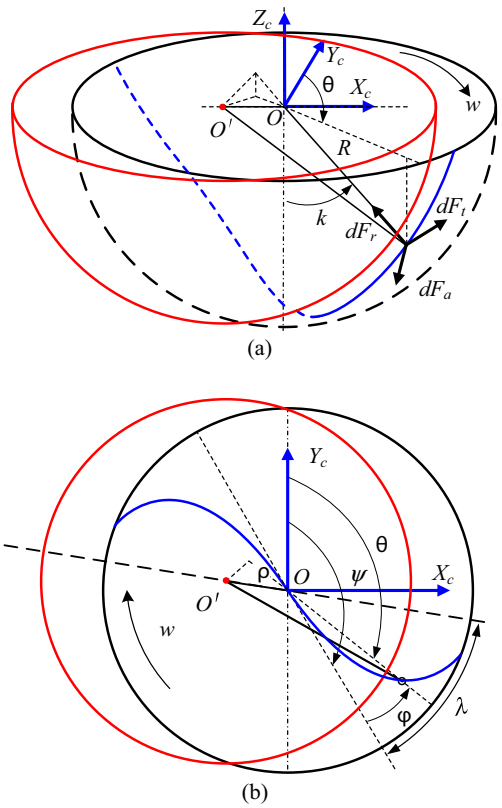

Fig. 5 The constant lead helical ball-end mill. **a** 3D graph. **b** Z_n-axial negative view

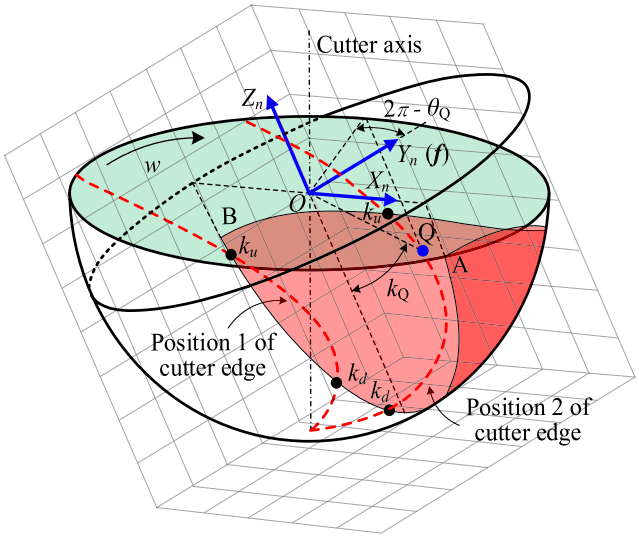

Fig. 6 ICCE

the CWE of the cutter contact normal coordinate system to judge whether Q (x_c y_c z_c) is involved in cutting.

The judgment conditions corresponding to the micro-cutter edge Q (x_n y_n z_n) are expressed as follows:

$$\begin{cases} 1) : 0 \le \theta_Q \le \theta_A \vee \theta_B \le \theta_Q \le 2\pi \\ 2) : k_{AB}(\theta_Q) \le k_Q(\theta_Q) \le k_{(AB)'}(\theta_Q) \end{cases} \tag{12}$$

where θ_A, θ_B, and θ_Q are the expressions of the radial position angles corresponding to points A, B, and Q in the cutter contact normal coordinate system, respectively. k_Q denotes the axial position angle of the micro-cutter edge Q (x_n y_n z_n). $k_{(AB)'}$ and k_{AB} denote the expressions of the corresponding axis position angles of the boundary curves (AB)' and AB in the cutter contact normal coordinate system at the radial position angle θ_Q, respectively. Compared with k_{AB}, $k_{(AB)'}$ is more difficult to solve. It is necessary to combine the sphere surface, to-be-machined surface and plane $\tan(\theta_Q) = x_n/y_n$ to derive $k_{(AB)'}$. The expressions are as follows:

$$\begin{aligned} &\theta_A = \pi; \quad \theta_B = 3\pi/2 \\ &\begin{cases} x_n \ge 0, y_n \ge 0 : \theta_Q = \arctan(x_n/y_n) \\ y_n \ge 0 : \theta_Q = \pi + \arctan(x_n/y_n) \\ x_n \le 0, y_n \ge 0 : \theta_Q = 2\pi + \arctan(x_n/y_n) \end{cases} \end{aligned} \tag{13}$$

$$\begin{aligned} &k_{AB}(\theta_Q) = 0 \\ &k_Q(\theta_Q) = \arccos(-z_n/R) \\ &k_{(AB)'}(\theta_Q) = \arccos\left(\sec^2\theta\left(\sqrt{T^2\sin^2\theta + (R')^2\cos^2\theta} - T\right)/R\right) \end{aligned} \tag{14}$$

Based on the judgment conditions of Eq. (12), starting from the tip of cutter edge, the micro-cutter edge is judged one by one along the cutter edge curve to find two consecutive points, one located on inside of CWE and the other on the outside. Dichotomous search method is used to gradually approach the precise lower point k_d between the two points. Then searching along the cutter edge curve continuously until the upper boundary point k_u of ICCE is determined.

The above algorithm can obtain the upper and lower bounds [k_u k_d] of ICCE of a cutter edge at any cutter rotation position angle. The ICCE of N_{th} cutter edge could be determined by increasing tooth pitch angle $2\pi/N$.

5 Model of the cutting force

Based on the classic oblique cutting theory [21], as shown in Fig. 5a, the tangential force $dF_{t,j}$, radial force $dF_{r,j}$, and axial force $dF_{a,j}$ of micro-cutter edge on cutter edge j at the axial position angle k are as follows:

$$\begin{cases} dF_{t,j}(\theta_j, k) = K_t t_n(\theta_j, k) db \\ dF_{r,j}(\theta_j, k) = K_r t_n(\theta_j, k) db \\ dF_{a,j}(\theta_j, k) = K_a t_n(\theta_j, k) db \end{cases} \tag{15}$$

where K_t, K_r, and K_a are tangential, radial, and axial cutting force coefficients, respectively. db is the chip width of the micro-cutter edge, expressed as Eq. (16).

The effective instantaneous chip layer thickness $t_n(\theta_j,k)$ of the micro-cutter edge consists of two parts. $t_{n1}(\theta_j,k)$ is defined by the projection component of feed per tooth f_c on the spherical surface normal of the micro-cutter edge k [22]. The cutter run-out theory of flat-end mill is extended to the ball-end mill, the model being shown in Fig. 5. $t_{n2}(\theta_j,k)$ is the chip layer thickness difference of the adjacent teeth caused by the cutter run-out. The expression is shown in Eq. (17).

$$db = Rdk \tag{16}$$

$$\begin{aligned} &t_{n1}(\theta_j, k) = f_c\cos\gamma\sin k\sin\theta_j + f_c\cos\eta\sin k\cos\theta_j - f_c\cos\xi\cos k \\ &t_{n2}(\theta_j, k) = -2\rho\sin k\sin(\pi/N)\sin(\lambda - \sigma) \qquad \sigma = \psi - \theta_j + (2j-3)\pi/N \end{aligned} \tag{17}$$

where η and ξ are the angles between the Y_c-axis and the Z_c-axis with the feed vector $\boldsymbol{f}$ respectively. The equations are as follows:

$$\begin{cases} \eta = \arccos\left(\dfrac{(\boldsymbol{p} \times (\boldsymbol{p} \times \boldsymbol{n}))g\boldsymbol{f}}{|\boldsymbol{p} \times (\boldsymbol{p} \times \boldsymbol{n})\|\boldsymbol{f}|}\right) \\ \xi = \arccos\left(\dfrac{\boldsymbol{p}g\boldsymbol{f}}{|\boldsymbol{p}\|\boldsymbol{f}|}\right) \end{cases} \tag{18}$$

The cutting forces in the x, y and z directions of the cutter coordinate system obtained by transformation are:

$$\begin{bmatrix} dF_{x,j}(\theta_j,k) \\ dF_{y,j}(\theta_j,k) \\ dF_{z,j}(\theta_j,k) \end{bmatrix} = \begin{bmatrix} -\cos\theta_j & -\sin k\sin\theta_j & \cos k\sin\theta_j \\ \sin\theta_j & -\sin k\cos\theta_j & \cos k\cos\theta_j \\ 0 & \cos k & \sin k \end{bmatrix} \begin{bmatrix} dF_{t,j}(\theta_j,k) \\ dF_{r,j}(\theta_j,k) \\ dF_{a,j}(\theta_j,k) \end{bmatrix} \tag{19}$$

Based on the above ICCE [k_u k_d] and integrating along the axial direction, the cutting forces acting on the cutter tooth j can be obtained as

$$\begin{bmatrix} F_{x,j}(\theta_j) \\ F_{y,j}(\theta_j) \\ F_{z,j}(\theta_j) \end{bmatrix} = \begin{bmatrix} \int_{k_d}^{k_u} dF_{x,j}(\theta_j,k) \\ \int_{k_d}^{k_u} dF_{y,j}(\theta_j,k) \\ \int_{k_d}^{k_u} dF_{z,j}(\theta_j,k) \end{bmatrix} \tag{20}$$

In the cutter coordinate system, the cutting forces in the direction of X_c-axis, Y_c-axis, and Z_c-axis of the cutter can be obtained by summing up the cutting forces on all the teeth.

$$\begin{bmatrix} F_{xc}(\psi) \\ F_{yc}(\psi) \\ F_{zc}(\psi) \end{bmatrix} = \begin{bmatrix} \sum_{j=1}^{N} F_{x,j}(\theta_j) \\ \sum_{j=1}^{N} F_{y,j}(\theta_j) \\ \sum_{j=1}^{N} F_{z,j}(\theta_j) \end{bmatrix} \tag{21}$$

In clean-up machining, most dynamometers are fixed on the workpiece. To facilitate measurement and analysis of milling forces, the three-dimensional instantaneous forces are regarded as spatial point set. The angle between the X_c-axis of the cutter coordinate system and the X_w-axis of the workpiece coordinate system is σ. The cutting forces in the workpiece coordinate system obtained by rotation transformation are:

$$[F_{xw} \quad F_{yw} \quad F_{zw}] = [F_{xc} \quad F_{yc} \quad F_{zc}]\boldsymbol{T}_p(\sigma) \qquad \boldsymbol{p} = (0 \quad 0 \quad 1) \tag{22}$$

where

$$\sigma = \arccos\left(\frac{\boldsymbol{w}\cdot\boldsymbol{p}}{|\boldsymbol{w}||\boldsymbol{p}|}\right) \tag{23}$$

where σ is a vector angle. When $\boldsymbol{w}\times\boldsymbol{p}$ points to the positive direction of the Z_w-axis, σ is positive, otherwise is negative.

6 Experiments and simulations of pencil-cut machining

In order to verify the validity of the CWE model, ICCE algorithm and the cutting force prediction model of pencil-cut machining with ball-mill established in this paper, a series of experiments and simulations were carried out. Two kinds of feed routes, pulling and pushing milling, were compared and analyzed in pencil-cut machining.

6.1 Comparison experiments of pulling and pushing milling for pencil-cut machining

The pulling and pushing milling respectively correspond to the front and back sides of the allowance section plane that is through the center of sphere. Since the position relationship between cutter axis and CCC is arbitrary, it is necessary to explore pulling and pushing milling for getting better machining effect.

The experimental workpiece is 45 steel, and the parameters such as coordinate system and workpiece size are shown in Fig. 7a. Pulling and pushing milling pencil-cut machining were performed in CCC 1 and 2, respectively. The radius of the to-be-machined arc is 5 mm. A dextral solid cemented carbide ball-end mill with 8 mm diameter, two flutes and 35° helix angle was used to cut. The protruding length of the cutter is 34 mm to avoid chatter. The tool paths were generated by using curves/points drive method of manufacture model of Unigraphics NX and the experiments were performed on the Dongtai CMV-850A Three-axis CNC Machining Center. Machining vibration and the cutting force were collected and analyzed by the YDCB-III005 three-dimensional piezoelectric quartz dynamometer, the DYTRAN 3035B accelerometer and INV3018A data acquisition analyzer of China orient institute of noise and vibration. The roughness of the machined surface was measured by Form Talysurf PGI 840 Hommel Roughness Tester. The processing parameters are shown in Table 1. In experiments 1–3, the tip of cutter did not participate in the pulling pencil-cut machining, while in the experiments 4–6, it participated in cutting. The condition of tool nose involved in pushing pencil-cut milling is:

$$\varepsilon \le \pi - \arccos\left(\left(T^2 + R^2 - \left(R'\right)^2\right)/(2RT)\right) \tag{24}$$

Experiments are shown in Fig. 7b. Water-based cutting fluid was used to cool. Comparison results of the milling force, surface roughness and vibration are shown in Table 1. The difference of the peak in a period of the force waveforms is caused by the cutter run-out and so on. Usually, the damage of the machining system depends on the maximum cutting force. It is measured by the average value of the maximum

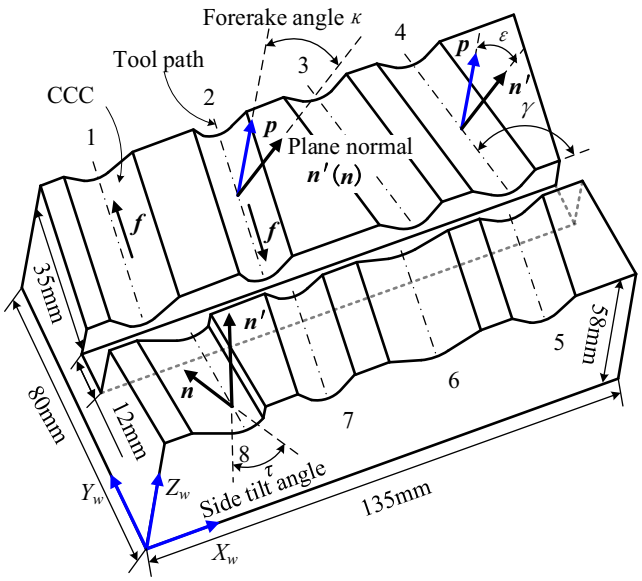

(a)

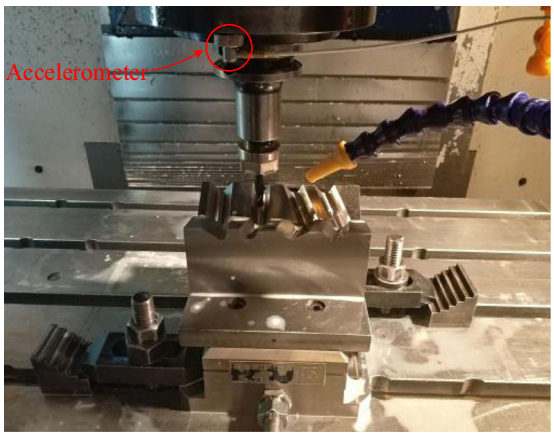

(b)

Fig. 7 Pencil-cut machining of ball-end mill. **a** Schematic diagram of workpiece. **b** The graph of processing site

wave peak in multiple consecutive periods of the cutting force. Three-axis cutting forces of pulling milling are obviously smaller than pushing milling in cutter coordinate system. Therefore, pulling milling has distinct advantages in reducing tool wear and tool deformation, prolonging tool life, as well as improving the geometric precision of the workpiece. As shown in Fig. 8, the roughness R_a is measured on the four sampling sections of the machined surface of CCC. The average value of roughness R_a in Tab. 1 indicates that the surface quality of pulling milling is better than pushing milling. The accelerometer was fixed on the top of the spindle. The effective value of the measured data can indirectly reflect the vibration degree in the milling process. The results also show that the processing stability of pulling milling is obviously better than pushing milling. In conclusion, the contrast experiments of pulling milling and pushing milling with different processing parameters show that the method of pushing milling should be preferential in the pencil-cut machining.

6.2 CWE and ICCE of CCC pencil-cut machining

In order to verify the correctness of the analytical model of CWE, a CWE experiment for the three-axis pencil-cut machining was carried out in the CCC 4. The radius of the arc surface to be machined is 5 mm, the tool diameter is 8 mm, the tilt angle of the cutter ε is 30°, the feed direction angle is 110°, and the cutting depth is 1 mm. Cutter lifted at (113.693 60.898 37.393) in workpiece coordination system along positive Z_c-axis. A clear boundary of CWE at the point was obtained.

The boundary of CWE obtained from the experiment was sampled along the Z_w-axis negative direction with the Digital Image Tools Microscope VTM-3020F. The workpiece coordinate system is set as the measurement coordinate system. Taking into account the accuracy of the solid modeling method, an accurate three-dimensional model of CWE can also be obtained by the intersection between the models of the cutter and workpiece in the same machining parameters with the Boolean operation command of the Unigraphics NX software modeling module. The comparison of CWE obtained by the solid modeling method, experiment, and MATLAB numerical analysis software based on the analytical theory of this paper

Table 1 Experimental parameters and results of pushing and pulling pencil-cut machining

No.	d_n (mm)	f (mm/min)	κ (degree)	S (r/min)	F_{xc} (N)		F_{yc} (N)		F_{zc} (N)		R_a (μm)		vibration (g)	
					Push	Pull	Push	Pull	Push	Pull	Push	Pull	Push	Pull
1	0.1	300	60	1000	142.4	94.1	− 108.5	63.04	− 49.2	− 14.2	2.5675	0.8882	0.126	0.096
2	0.3	200	60	1000	195.7	144.4	− 177.7	105.2	− 82.7	16.4	0.9032	0.5055	0.144	0.103
3	0.5	150	60	1000	234.7	173.4	− 224.3	148.1	− 124.7	18.5	1.0774	0.4938	0.160	0.096
4	0.6	100	15	2000	− 102.9	144.5	135.1	164.9	− 351.2	− 133.8	1.2003	0.1902	0.268	0.196
5	0.8	70	15	2000	− 137.7	136.5	197.9	128.5	− 260	− 109.2	0.4331	0.0976	0.202	0.147
6	1	50	15	2000	− 138.3	117.8	198.5	122.2	− 225	− 120.1	0.9202	0.0828	0.244	0.193

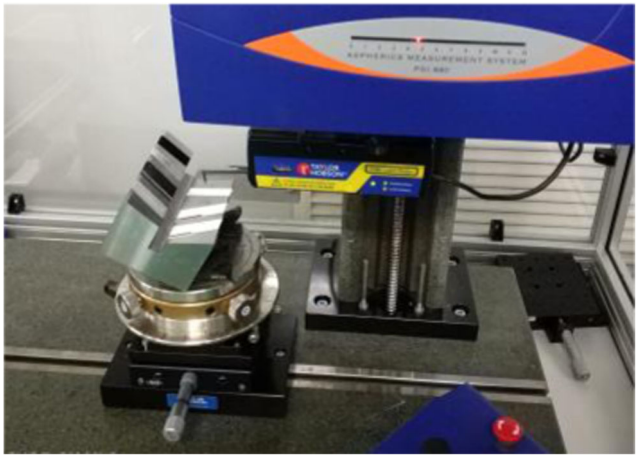

Fig. 8 Roughness measurement of the machined surface

is shown in Fig. 9. CWE obtained by the analytical method and the solid modeling method agree well with each other, while there are some deviations in the comparison with the experimental result. Considering the factors, such as the machining error, tool-setting error, measurement error, tool run-out, and the unclear boundary curve AB leaded by friction, it is effective to prove the correctness of the analytical model of CWE in this paper by the experiment and solid simulation.

With machining parameters of the above experiment, the trend of the upper and lower boundary points of the ICCE obtained by the presented algorithm is shown in Fig. 10. It is

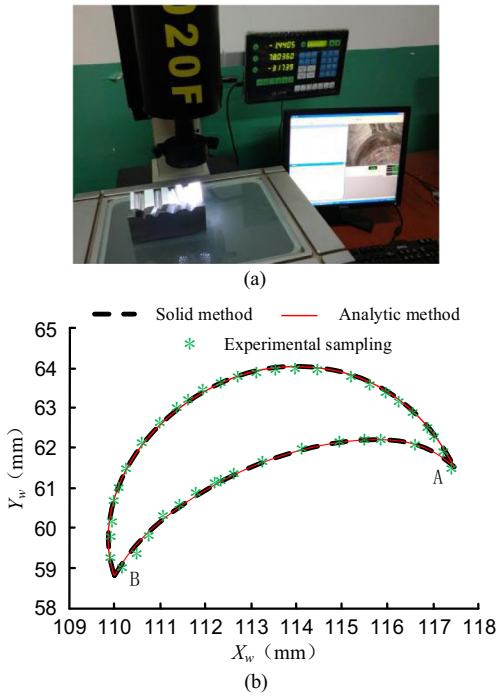

Fig. 9 Experiment of CWE for pencil-cut machining. **a** Tools microscope. **b** Comparison of three methods for CWE

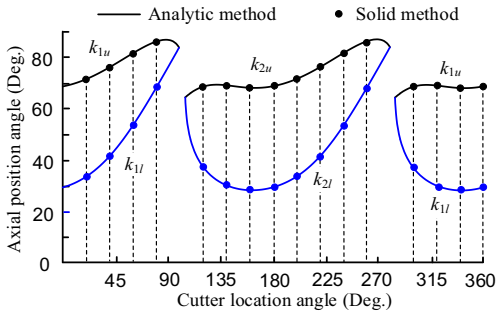

Fig. 10 Simulation of ICCE for pencil-cut machining

considered that the solid modeling method based on Unigraphics NX software is absolutely accurate. After modeling and performing Boolean operation for CCC, tool geometry and cutter edge curve, the upper and lower boundary points of ICCE, at cutter location angles 20°, 40°, 60°, 80°, 120°, 140°, 160°, 180°, 200°, 220°, 240°, 260°, 300°, 320°, 340°, and 360°, were obtained, respectively. The simulation shows that the two results are completely consistent, which proves the correctness of the proposed algorithm of ICCE. The analytic algorithm ran on a personal computer with the processor: Intel(R) Core(TM) i5-7500 CPU @ 3.40 Hz 3.41 Hz, RAM: 8.00 GB. Operating time is 0.187463 s. It shows the advantages of high efficiency and high accuracy.

6.3 Cutting force prediction of CCC pencil-cut machining

In order to validate the cutting force model, a series of pencil-cut experiments were performed where the feed direction and the processing parameters were arbitrary. Workpiece, tool parameters, machine tools, force measurement systems, and tool path planning method are described in experiments of pushing and pulling machining. The machining site is shown in Fig. 7b.

Cutting force coefficients are crucial for the accuracy of the cutting force prediction. Based on the method of cutting force coefficients identification of the flat-end mill established by Wei et al. [23], eight experiments of single-tooth cutting coefficients identification were carried out on the CCC 1 and 2, and the machining parameters are shown in Table 2. The cuter forerake angle κ and the side tilt angle τ were selected by the processing and programming module of Unigraphics NX. The relationship between the both angles and tool axis tilt angle ε is shown in Eq. (25).

$$\cos\varepsilon = \cos\kappa\cos\tau \tag{25}$$

Table 2 Experimental parameters of coefficients identification

d_n (mm)	R' (mm)	κ (degree)	τ (degree)	f (mm/r)	S (r/min)
1	8	10~45 ($\Delta = 5°$)	0	180	500

For the measured instantaneous average cutting force corresponding to N teeth, combining the corresponding axial position angle $k^{'}$ and the chip layer thickness $t_n^{'}$, after substituting them into the cutting force prediction model, the corresponding three-direction cutting force coefficients were obtained by the method of undetermined coefficients. The surface of discrete coefficient point set was fitted using MATLAB's Curve Fitting Tool. The polynomial expression of fitted surface of cutting force coefficients K_t, K_r and K_a as Eq. (26), polynomial coefficients are shown in Table 3. Based on the instantaneous measured force of any single cutter edge and the cutting force coefficients, the cutter run-out parameters were back-calculated. Taking the axial inclination angle 30° as an example, the run-out distance ρ and the run-out angle λ are shown in Eq. (27).

$$K_v = p_0 + p_1 x + p_2 y + p_3 x^2 + p_4 xy + p_5 y^2 + p_6 x^3 + p_7 x^2 y + p_8 xy^2 + p_9 y^3 \quad \left(v = t, r, a; \quad x = k^{'}, y = t_n^{'}\right) \tag{26}$$

$$\varepsilon = 30^{\circ}: \quad \rho = 0.0115\text{mm}; \quad \lambda = 110.374^{\circ} \tag{27}$$

A large number of experiments with variable processing parameters and variable cutter axis vector were conducted on the CCC 3–8. Some parameters are shown in Table 4. According to the relevant theory of Wan et al. [24], the spindle speed was set to 500 r/min to avoid chatter. Based on the above cutting force coefficients and the presented pencil-cut cutting force prediction model, a series of machining experiments were carried out to predict the cutting force. Since the distribution of the CCC on the workpiece is distinct from each other, the cutting forces were translated into cutter contact point normal coordinate system O-$x_n y_n z_n$ by the Eq. (22) to facilitate the analysis of the forces and the sum of the laws. The comparisons of the measured cutting forces with the predicted cutting forces are shown in Fig. 11.

The influences of cutter run-out on the cutting-in and cutting-out angle of the cutter edge are not considered to simplify the prediction model of cutting force in this paper, which result in a little asynchronism between the measured forces and the predicted forces in the time domain. As shown in the marker of graph. The cutting force coefficients identification is based on the left part of the measured cutting forces corresponding to the monotone interval of the instantaneous average chip layer thickness. When the coefficients are used to predict the cutting force of the entire region, because of the difference of the down and up milling in left and right parts of the cutting region, there is a larger amplitude error at the right side of trough of F_{yn} [25]. Meanwhile, in the coefficients identification experiments of this paper, there is a lesser Z_c-axial force of the cutter coordinate system when the cutter forerake angle is large. It is easy to suffer the external jamming, which affects the accuracy of coefficients identification. In the cutting force coefficients fitting surface, the sampling points are deficient in where the instantaneous chip layer thickness and the axial position angle are small. The cutting depth is large so that the estimation of the average axial position angle is rough. Above reasons result in the inaccurate coefficients identified in this paper, further lead to deviation between the predicted force and measured force. The maximum error between the measured and the predictive forces in this experiment is about 20%. In short, taking into account the factors, such as the identification error of cutting coefficients, the roughness of micro-milling force model, machining errors, etc. the series of experiments can effectively demonstrate the correctness of the prediction model of the cutting force for pencil-cut machining of ball-end mill established in this paper.

Table 4 Experimental parameters of pencil-cut machining

No.	d_n (mm)	$R^{'}$ (mm)	κ (degree)	τ (degree)	f (mm/r)
1	1	16	20	0	180
2	1	16	40	0	180
3	0.6	16	30	0	180
4	1	13	30	0	180
5	1	16	30	0	120
6	1	16	30	5	180

Table 3 Polynomial coefficients of K_t, K_r, K_a ($\times 10^4$)

Coefficients	P_0	P_1	P_2	P_3	P_4	P_5	P_6	P_7	P_8	P_9
K_t	− 1.47	2.84	2.00	− 1.07	− 63.8	667	− 0.431	44.7	− 188	− 4240
K_r	0.728	− 2.26	− 31.1	2.05	16.9	665	− 0.982	19.4	− 555	− 1940
K_a	− 0.67	1.34	20.7	− 0.903	− 14.5	− 377	0.204	1.32	190	1270

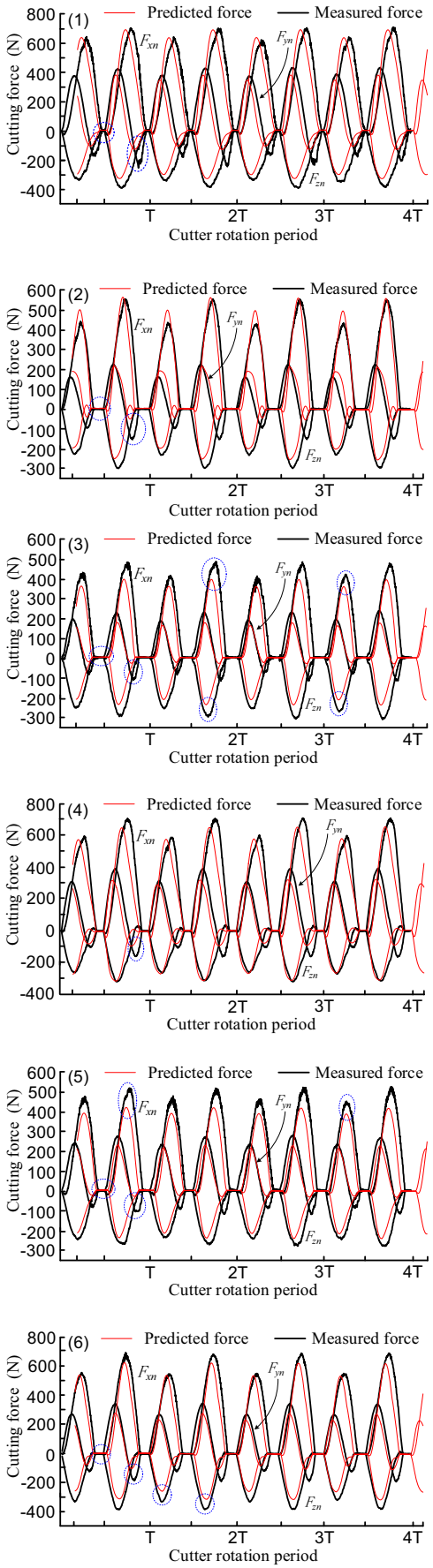

◀ **Fig. 11** Measured and predicted cutting forces of pencil-cut machining

7 Conclusion

Aiming at pencil-cut machining of concave crescent cylindrical (CCC), the cutter coordinate system, the cutter axis tilt angle, and the feed direction angle are defined. Parametric expressions of the relationships between the cutter axis vector, the feed direction and the CCC are achieved.

Taking the pencil-cut machining of ball-end cutter in CCC as the research object, the cutter, the cutter sweep surface, and the surface to be machined are analytically expressed in the cutter contact point normal coordinate system. The analytical expressions of the boundary curves of CWE are obtained by intersecting surfaces. Using the space rotation transformation between coordinate systems, an analytical model of CWE in the cutter coordinate system is established.

The cutter edge curve is discretized into a series of micro-cutter edge. Based on the CWE above, the conditions of the micro-cutter edge in the CWE are proposed, that is, the conditions being in cutting. The upper and lower boundaries of ICCE are found one by one along the edge curve. Further, the accuracy of boundary points can be improved by dichotomy.

Based on the analytical algorithm of ICCE, combined with the micro-unit cutting force of the ball-end mill and the theory of the chip layer thickness considering cutter run-out, a prediction model of the cutting force for pencil-cut machining of CCC with ball-end mill is established.

In this paper, a series of simulations and experiments of pencil-cut machining of CCC were carried out. Compared with pushing milling, pulling milling is better in the terms of cutting force, surface roughness, and machining stability. The analytical model agrees reasonably with both the experimental results and the solid simulation results of CWE, also the ICCE obtained by the solid modeling method are consistent with the analytical algorithm. A series of experiments prove the correctness of the prediction model of the cutting force for pencil-cut machining of ball-end mill.

Funding information This research is supported by the Natural Science Foundation of Liaoning No. 201602174 and the Fundamental Research Funds for the Central Universities No. DUT17GF213.

References

1. Zhang X, Zhang J, Zhao WH (2016) A new method for cutting force prediction in peripheral milling of complex curved surface. Int J Adv Manuf Technol 86(1–4):117–128
2. Huang T, Zhang X, Ding H (2013) Decoupled chip thickness calculation model for cutting force prediction in five axis ball-end milling. Int J Adv Manuf Technol 69(5–8):1203–1217

3. Yun WS, Cho DW (2000) An improved method for the determination of 3D cutting force coefficients and runout parameters in end milling. Int J Adv Manuf Technol 16(12):851–858
4. Park SC, Choi BK (2001) Uncut free pocketing tool-paths generation using pair-wise offset algorithm. Comput Aided Des 33(10): 739–746
5. Choy HS, Chan KW (2003) A corner-looping based tool path for pocket milling. Comput Aided Des 35(2):155–166
6. Pateloup V, Duc E, Ray P (2004) Corner optimization for pocket machining. Int J Mach Tools Manuf 44(12–13):1343–1353
7. Bouaziz Z, Zghal A (2008) Optimization and selection of cutters for 3D pocket machining. Int J Comput Integr Manuf 21(1):73–88
8. Guerrero-Villar F, Dorado-Vicente R, Romero-Carrillo P, López-García R, Mercado-Colmenero J (2015) Computation of instantaneous cutter engagement in 2.5D pocket machining. Procedia Engineering 132:464–471
9. Zhang L, Zheng L (2004) Prediction of cutting forces in milling of circular corner profiles. Int J Mach Tools Manuf 44:225–235
10. Kris AG, Law MY, Geddam A (2001) Prediction of contour accuracy in the bed milling of pockets. J Mater Process Technol 113(1–3):399–405
11. Dotcheva M, Millward H (2005) The application of tolerance analysis to the theoretical and experimental evaluation of a CNC corner-milling operation. J Mater Process Technol 170:284–297
12. Bae SH, Ko K, Bo HK, Choi BK (2003) Automatic federate adjustment for pocket machining. Comput Aided Des 35(5):195–500
13. Peng C, Wang L, Li Z, Yang Y (2014) Time-domain simulation and experimental verification of dynamic cutting forces and chatter stability for circular corner milling. Proc Inst Mech Eng B J Eng Manuf 229:932–939
14. Ren Y, Yau HT, Lee YS (2004) Clean-up tool path generation by contraction tool method for machining complex polyhedral models. Comput Ind 54:17–33
15. Kim DS, Jun CS, Park S (2005) Tool path generation for clean-up machining by a curve-based approach. Comput Aided Des 37:967–973
16. Tang M, Zhang D, Luo M, Wu B (2012) Tool path generation for clean-up machining of impeller by point-searching based method. Chin J Aeronaut 25:131–136
17. Zhu W, Lee YS (2004) Five-axis pencil-cut planning and virtual prototyping with 5-DOF haptic interface. Comput Aided Des 36(13):1295–1307
18. Ding YP, Liu XL, Shi HN, Li J, Zhang R (2014) Modeling and simulation of ball end milling force for mold cavity corner. Mater Sci Forum 800-801:337–341
19. Yue CX, Huang C, Liu XL, Hao SY, Liu J (2017) 3D FEM simulation of milling force in corner machining process. Chin J Mech Eng 30(2):286–293
20. Wei ZC, Wang MJ, Cai YJ, Wang SF (2013) Prediction of cutting force in ball-end milling of sculptured surface suing improved Z-map. Int J Adv Manuf Technol 68(5–8):1167–1177
21. Guo ML, Wei ZC, Wang MJ, Li SQ, Liu SX (2018) Force prediction model for five-axis flat end milling of free-form surface based on analytical CWE. Int J Adv Manuf Technol. https://doi.org/10.1007/s00170-018-2480-1
22. Wei ZC, Guo ML, Wang MJ, Li SQ, Liu SX (2018) Force predictive model for five axis ball end milling of sculptured surface. Int J Adv Manuf Technol 98(5–8):1367–1377
23. Wei ZC, Guo ML, Wang MJ, Li SQ, Liu SX (2018) Prediction of cutting force in five-axis flat end milling. Int J Adv Manuf Technol 96(1–4):137–152
24. Wan M, Ma CY, Zhang WH, Yang Y (2015) Study on the construction mechanism of stability lobes in milling process with multiple modes. Int J Adv Manuf Technol 79(1–4):589–603
25. Guo ML, Wei ZC, Wang MJ, Li SQ, Liu SX (2018) An identification model of cutting force coefficients for five-axis ball end milling. Int J Adv Manuf Technol. https://doi.org/10.1007/s00170-018-2451-6